DOI: 10.61782/fa.2023.0181

forum acusticum 2023

OPTIMAL SHAPING OF RECTANGULAR ACOUSTIC BLACK HOLES FOR SOUND ABSORPTION IN AIR

Milan Červenka*, **Michal Bednařík**
Czech Technical University in Prague, Faculty of Electrical Engineering
Technická 2, 166 27, Prague 6, Czech Republic

ABSTRACT

In this work, we examine the performance of rectangular acoustic black holes (ABHs) serving as an anechoic termination in air-filled waveguides. These ABHs, consisting of rigid ribs separated by narrow slits with varying heights, are designed to slow down and absorb impinging acoustic waves. A one-dimensional mathematical model, employing the Riccati equation, is used for the numerical calculations. It accounts for the attenuation of acoustic energy in the thermo-viscous boundary layer through the use of an equivalent fluid model. The accuracy of this simplified, but computationally efficient model is verified by comparing its results to those obtained from a two-dimensional simulation using linearized Navier-Stokes equations and the finite element method. To optimize the ABH profile for maximum acoustic energy absorption, a genetic algorithm is employed in conjunction with the simplified mathematical model. The results demonstrate that the ABHs with an optimized profile exhibit superior performance compared to those with a non-optimized profile, but otherwise the same internal structure.

Keywords: *rectangular acoustic black hole, Riccati equation, shape optimization, genetic algorithm.*

1. INTRODUCTION

The concept of an acoustic black hole (ABH) serving as an anechoic termination of a gas-filled duct was introduced in 2002 by Mironov and Pislyakov [1]. In their paper, the authors studied the properties of a retarding structure formed by a piece of tapered tube with varying wall admittance. Employing an analytical solution of the corresponding wave equation, they have demonstrated that if the tube radius reduces to zero as a linear function of the axial coordinate and if the tube wall-admittance has a certain functional form, the wave speed at the tube apex reduces to zero. This way, at least in theory, the acoustic wave cannot reach the apex in a finite time, which means that it cannot be reflected back into the waveguide and stays trapped in the structure. The required wall admittance, as proposed in [1], can be, in theory, introduced by a set of circular ribs separated by narrow slits whose inner radii reduce to zero towards the structure apex and which form the inner wall of the tube.

In subsequent theoretical works [2, 3], the behavior of ABHs with quadratic radius profile has been modeled employing the transfer matrix method (TMM). The effect of ABH has also been studied experimentally [4–7], and various modifications and applications of ABHs have also been explored [8–10]. It has recently been noticed [7, 11, 12] that the acoustic energy absorption in the structure proposed by Mironov and Pislyakov [1] is not primarily connected with the acoustic wave slow-down; it is rather caused by resonances taking place in the cavities between the ribs, resembling the rainbow trapping [13]. Despite this fact, we will refer to these absorbers as acoustic black holes, because this term has already been used in connection with these structures.

All the structures studied in the previously-referred works have one common property, i.e. an axial symmetry, which makes them suitable to serve as an anechoic termination for ducts with a circular cross-section. However, in many cases, the ductwork, e.g., in HVAC systems, possesses rectangular cross-section.

**Corresponding author*: milan.cervenka@fel.cvut.cz.

The aim of this work is to explore the absorbing properties of ABHs similar to the ones proposed in [1], however, having a rectangular shape. Special attention is put to these questions: What is the optimum ABH shape? How does it depend on the other parameters? The paper is organized as follows. The employed mathematical model, parametrization of the ABH shape, quantification of its performance, and the numerical procedure are outlined in Sec. 2. The numerical results are presented in Sec. 3, some concluding remarks are then given in Sec. 4.

2. MATHEMATICAL MODEL

The ABH terminating a waveguide with a rectangular internal cross-section $2A \times B$ (height $\times$ width), where $B \leq 2A$, is schematically depicted in Fig. 1. It consists of a set of N pairs of opposing rigid ribs spanning the width B of the waveguide. The ribs are attached to the top and bottom wall of the waveguide and their heights $h(x_i) = A - a(x_i)$ smoothly vary along the structure whose total length is L. Here, x_i represents the position of the i-th rib, and $a(x)$ is the ABH's shape function defining its profile. The heights of the opposing ribs forming a pair is always the same. The separation distance between the centers of the neighboring ribs is $H = L/N$, the width of the cavities (slits) between them is set as $h = \xi H$, where $\xi \in (0, 1)$. It means that the width of the ribs $h_{\text{rib}} = H - h = (1 - \xi)H$. The detail of the ABH internal geometry is schematically depicted in Fig. 2.

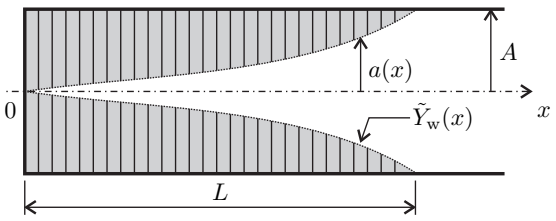

Figure 1. Model of a rectangular acoustic black hole.

The end of the structure is terminated with a rigid wall. The aim of the structure is to absorb the acoustic plane wave impinging from the right side from the waveguide which is assumed to be infinite.

As all the calculations are conducted at frequencies below the cut-on frequency of the waveguide

$$f_{\text{cut-on}} = \frac{c_0}{4A},$$

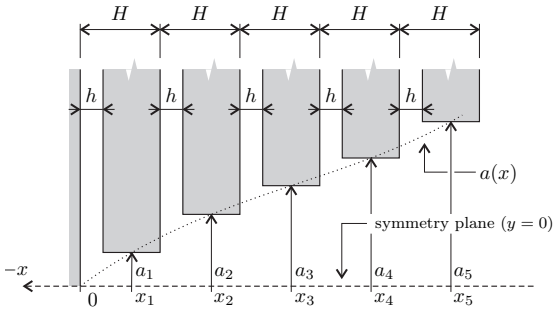

Figure 2. Detail of the internal structure of an acoustic black hole.

where c_0 is the sound speed, all the acoustic-field quantities inside the ABH are assumed to be only functions of the longitudinal spatial coordinate x.

2.1 Riccati equation

Within this work, similarly as in [7], acoustic properties of ABHs are studied employing the Riccati equation for acoustic admittance $\tilde{Y}$, which can be, assuming an implicit time dependence $\mathrm{e}^{\mathrm{i}\omega t}$, written as

$$\frac{\mathrm{d}\tilde{Y}}{\mathrm{d}x} = \mathrm{i}\omega\tilde{\rho}_{0\mathrm{g}}\tilde{Y}^2 - \frac{\mathrm{i}\omega}{\tilde{\rho}_{0\mathrm{g}}\tilde{c}_{0\mathrm{g}}^2} - \frac{1}{a}\frac{\mathrm{d}a}{\mathrm{d}x}\tilde{Y} - \frac{\tilde{Y}_{\text{w}}}{a}, \qquad (1)$$

where $\omega = 2\pi f$ is the angular frequency, $\mathrm{i} = \sqrt{-1}$ is the imaginary unit, $\tilde{\rho}_{0\mathrm{g}}$, $\tilde{c}_{0\mathrm{g}}$ are effective complex ambient density and sound speed accounting for the boundary-layer losses in the ABH's main waveguide. These quantities are calculated employing the Stinson's model [14] for a slit with the width $2a$. Note that in this case $a = a(x)$, so that $\tilde{\rho}_{0\mathrm{g}} = \tilde{\rho}_{0\mathrm{g}}(x)$, and $\tilde{c}_{0\mathrm{g}} = \tilde{c}_{0\mathrm{g}}(x)$.

The wall admittance $\tilde{Y}_{\text{w}}(x)$, formed by the ends of the ribs and interjacent slits is set as

$$\tilde{Y}_{\text{w}}(x) = \frac{\mathrm{i}\xi}{\tilde{\rho}_{0\mathrm{s}}\tilde{c}_{0\mathrm{s}}} \tan\left\{\frac{\omega}{\tilde{c}_{0\mathrm{s}}}\left[A - a(x)\right]\right\}, \qquad (2)$$

where $\tilde{\rho}_{0\mathrm{s}}$, $\tilde{c}_{0\mathrm{s}}$ are effective complex ambient density and sound speed accounting for the boundary-layer losses in the slits of width h, as before, the Stinson's model is used.

The Riccati equation (1) is numerically integrated with initial condition $\tilde{Y}(x = 0) = 0$, representing the rigid wall terminating the ABH, in the interval $x \in \langle 0, L\rangle$. This way, the ABH input acoustic admittance $\tilde{Y}_{\text{ABH}} = \tilde{Y}(L)$ is determined. As it is assumed that the characteristic acoustic admittance of the infinite waveguide in front

of the ABH $Y = 1/\rho_0 c_0$, the reflection coefficient from the ABH is

$$\mathcal{R} = \frac{A + \rho_0 c_0 a_{\text{ABH}} \tilde{Y}_{\text{ABH}}}{A - \rho_0 c_0 a_{\text{ABH}} \tilde{Y}_{\text{ABH}}} \mathrm{e}^{2\mathrm{i}\omega L/c_0}, \tag{3}$$

where $a_{\text{ABH}} = a(L)$.

2.2 ABH shape parametrization

Throughout this work, the ABH profile is introduced as

$$a(x) = (A - A_{\text{min}}) G(x/L) + A_{\text{min}}, \tag{4}$$

where A_{min} is the minimum half-width of the ABH (at $x = 0$), and $G(X)$ is the shape-function meeting the condition $0 \leq G(X_0) \leq 1, \forall X_0 \in \langle 0, 1 \rangle$.

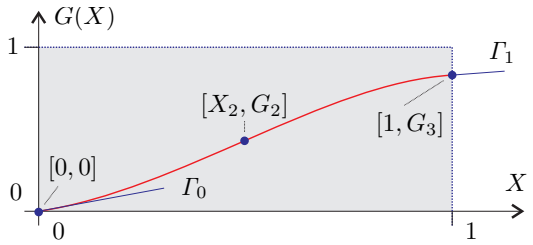

Figure 3. ABH shape function defined using three control points interconnected with cubic splines.

In order to introduce a wide variability in the shape-function, it was introduced employing the cubic splines interconnecting three control points having the coordinates $[X_i, G(X_i)] = [[0, 0], [X_2, G_2], [1, G_3]]$, see Fig. 3. Also, tangents at the extremities of the ABH were used as free parameters, namely,

$$\Gamma_0 = \frac{\mathrm{d}G}{\mathrm{d}X}\Big|_{X=0}, \qquad \Gamma_1 = \frac{\mathrm{d}G}{\mathrm{d}X}\Big|_{X=1}.$$

This means that the ABH shape was parametrized employing a five-component parameter vector

$$\boldsymbol{Z} = \{\Gamma_0, X_2, G_2, G_3, \Gamma_1\}.$$

2.3 Optimization procedure

As a quantifier of ABH's absorbing performance–the objective function for the optimization procedure, mean value of the modulus of the reflection coefficient (MRC) was introduced as

$$\text{MRC} = \frac{1}{f_{\text{cut-on}}} \int_0^{f_{\text{cut-on}}} |\mathcal{R}(f)| \, \mathrm{d}f, \tag{5}$$

where the reflection coefficient at individual discrete frequencies f_i was calculated using Eq. (3), and integral (5) was approximated employing the trapezoidal rule.

The ABH shape optimization was implemented as the search for a parameter vector $\boldsymbol{Z}$ minimizing the MRC function (5). For this purpose, genetic algorithm implemented in the MATLAB's Global Optimization Toolbox [15] was used.

3. NUMERICAL RESULTS

3.1 Parameters of the numerical simulations

In all the numerical simulations, the height of the rectangular waveguide and the ABH was set to $2A = 6\,\text{cm}$, and the parameter $\xi = 0.5$.

The fluid filling the waveguide and ABH is assumed to be air at normal conditions with the following material parameters: the sound speed $c_0 = 343.2\,\text{m}\,\text{s}^{-1}$, the ambient density $\rho_0 = 1.204\,\text{kg}\,\text{m}^{-3}$, the adiabatic exponent $\gamma = 1.4$, the dynamic viscosity $\mu = 1.83 \times 10^{-5}\,\text{Pa}\,\text{s}$, the specific heat capacity at constant pressure $c_\text{p} = 1004\,\text{J}\,\text{kg}^{-1}\,\text{K}^{-1}$, and the thermal conductivity $\kappa = 2.59\,\text{W}\,\text{m}^{-1}\,\text{K}^{-1}$. For these conditions, the cut-on frequency $f_{\text{cut-on}} = 2860\,\text{Hz}$.

3.2 Parametric study

Top panel of Fig. 4 shows the shape function of ABH optimized for parameters $L = 25\,\text{cm}$, $N = 500$, $A_{\text{min}} = 0.25\,\text{mm}$, and for the comparison, the shape functions of a linear $[G(X) = X]$, and quadratic $[G(X) = X^2]$ ABHs. It can be observed that the optimized shape features rather long contraction at the end of the ABH, and non-unity value of the shape function at the beginning of the ABH $[G(1) = 0.962]$. Also, the derivatives $\mathrm{d}G/\mathrm{d}X$ are close to zero at the extremities of the optimized ABH.

Bottom panel of Fig. 4 shows the reflection coefficient spectra of these ABHs, together with the values of MRC in the figure legend. It can be observed that the optimized ABH provides the smallest reflection coefficient in almost entire frequency range, especially at the lowest and the highest frequencies, and its MRC = 0.125 is also the lowest one. What is interesting is the fact that the rectangular ABH with linear profile performs rather poorly, which is in a strong contradiction with the case of an axisymmetric ABH with linear profile, which absorbs efficiently in the entire frequency range, see [12].

Top panel of Fig. 5 shows the shape functions of ABHs optimized for parameters $L = 25\,\text{cm}$, $N = 500$,

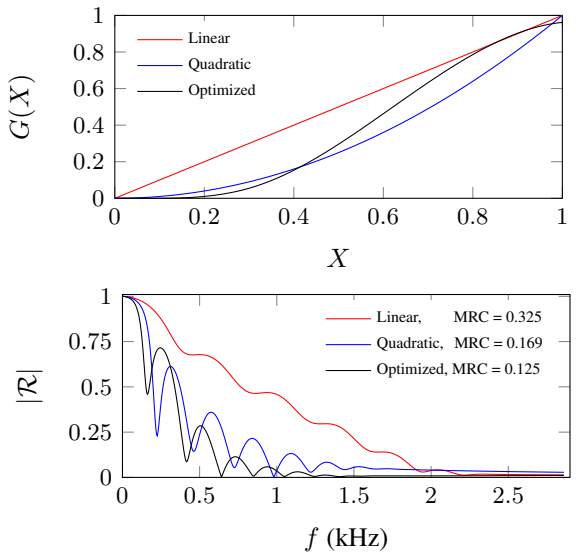

Figure 4. Top panel: shape function of an optimized, linear, and quadratic ABH; bottom panel: reflection coefficient spectra of optimized, linear, and quadratic ABH; $L = 25\,\text{cm}$, $N = 500$, $A_{\text{min}} = 0.25\,\text{mm}$.

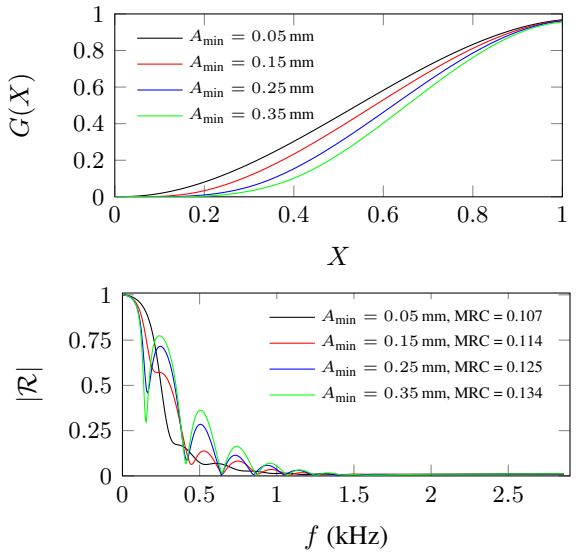

Figure 5. Top panel: shape functions of optimized ABHs with different values of A_{min}; bottom panel: corresponding reflection coefficient spectra; in all the cases, $L = 25\,\text{cm}$, $N = 500$.

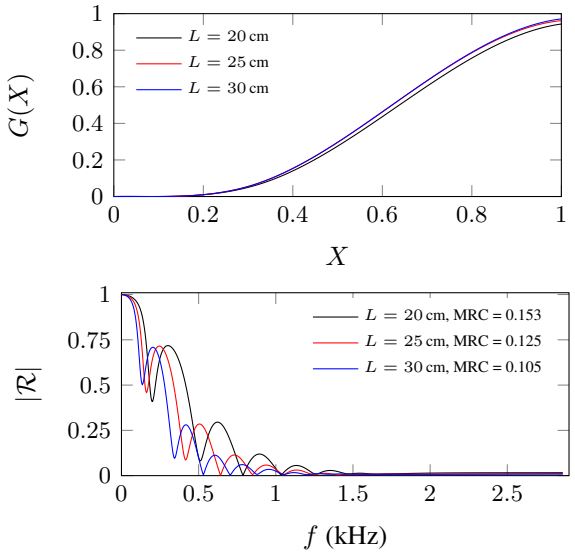

Figure 6. Top panel: shape functions of optimized ABHs with different values of L; bottom panel: corresponding reflection coefficient spectra; in all the cases, $N = 500$, $A_{\text{min}} = 0.25\,\text{mm}$.

and different values of A_{min}. It can be observed that the shape function depends on A_{min}, with its increasing value, the length of the most contracted part of the ABH increases.

The bottom panel of Fig. 5 shows the reflection coefficient spectra of these ABHs, together with the values of MRC in the figure legend. It can be observed that the value of MRC decreases with the value of A_{min}; the smaller the value of A_{min}, the less oscillatory the reflection coefficient spectrum is. On the other hand, an increased value of A_{min} results in the decrease of the reflection coefficient at the very low frequencies.

Top panel of Fig. 6 shows the shape functions of ABHs optimized for parameters $N = 500$, $A_{\text{min}} = 0.25\,\text{mm}$, and different lengths L. It can be observed that the optimum shape functions are rather similar, however, the lower the length L, the lower the value of $G(1)$.

The bottom panel of Fig. 6 shows the reflection coefficient spectra of these ABHs, together with the values of MRC in the figure legend. It can be observed that with the increasing value of the ABH length, the minima and maxima of the reflection coefficient spectrum shift towards the lower frequencies, and as a result, the greater the ABH

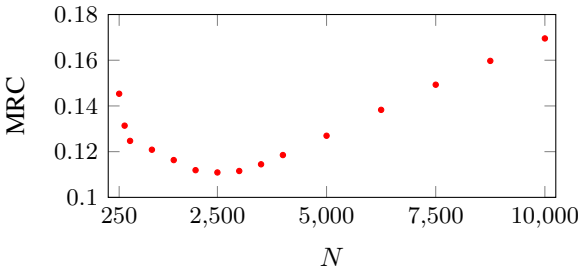

Figure 7. The value of MRC for optimized ABHs as a function of the number of ribs N; in all the cases, $L = 25\,\text{cm}$, and $A_{\text{min}} = 0.25\,\text{mm}$.

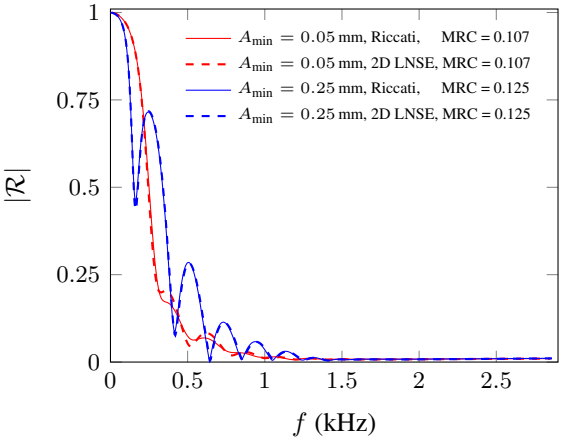

Figure 8. Comparison of the numerical results: reflection coefficient spectra calculated using the Riccati equation and 2D model based on the linearized Navier-Stokes equations (LNSE); in all the cases, $L = 25\,\text{cm}$, and $N = 500$.

length L, the lower the value of MRC.

Another question is: What is the optimal number of ribs for the given parameters to minimize the reflection from the ABH? Figure 7 shows the value of MRC as a function of N for optimized ABHs with $L = 25\,\text{cm}$, and $A_{\text{min}} = 0.25\,\text{mm}$. It can be observed that there is the minimum value of MRC = 0.111 for $N = 2500$.

Even if the ABH with the rib/slit spatial period $H = 0.1\,\text{mm}$ (corresponding to $L = 25\,\text{cm}$ and $N = 2500$) is hard to manufacture employing, for example, the contemporary 3D printing techniques, this result indicates that the performance of rectangular ABHs improves if their internal structure is fine. Moreover, the minimum of the dependence MRC(N) is rather wide and shallow.

3.3 Validation of the numerical results

All the numerical results presented within this work were obtained using the simplified one-dimensional model presented in Sec. 2.1. This model does not resolve the individual ribs and slits, nor it accounts for such effects as evanescent coupling of adjacent slits, or end-effects at the interfaces between the slits and the main ABH cavity. That is why the numerical results obtained employing the simplified model should be validated by comparison with numerical results calculated using a more accurate model. For this reason, two-dimensional model based on the linearized Navier-Stokes equations (LNSE) and finite element method (FEM), similar to the one proposed in our previous work [12], was used.

The comparison can be seen in Fig. 8 for the case of the reflection coefficient spectra of ABHs optimized for $L = 25\,\text{cm}$, $N = 500$, and $A_{\text{min}} = 0.05\,\text{mm}$ and $A_{\text{min}} = 0.25\,\text{mm}$, respectively. It is evident that the corresponding numerical results match to each other quite well; however, there are small discrepancies in the case of $A_{\text{min}} = 0.05\,\text{mm}$ in the mid-frequency range. What is interesting, see the legend in Fig. 8, is the fact that both the models predict the same value of MRC for the given value of A_{min}.

It can be thus concluded that the accuracy of the one-dimensional model employing the Riccati equation is reasonable for the purpose of the optimization of rectangular ABHs.

4. CONCLUSIONS

Within this work, we have studied the absorbing performance of rectangular ABHs serving as an anechoic termination in rectangular ducts. For this purpose, we used a computationally efficient one-dimensional mathematical model employing the Riccati equation, whose results were validated by comparison with a more accurate two-dimensional model employing the linearized Navier-Stokes equations and the finite element method. In contrast with the previously-published works, we have searched for an optimum ABH shape. For this purpose, we parametrized the ABH shape using control points interconnected with cubic splines and quantified the ABH performance using the mean value of the modulus of the reflection coefficient. The numerical results show that the ABH optimum shape slightly depends on the other

geometrical parameters; it is relatively simple, features close-to-zero derivatives at the ABH extremities, and has a relatively long contracted segment near the ABH apex. The optimal ABH profiles differ from simple power-law shapes studied in the previous works. The numerical results also show that the absorbing performance of rectangular ABHs increases with the decreasing value of the maximum profile contraction, increasing total length, and that there is an optimum number of ribs forming the ABH. Acoustic black holes seem to represent an innovative and unconventional means of implementing an anechoic termination of ductwork. As they do not employ fibrous materials, they can be used in harsh conditions where the working medium is hot, wet, dirty, greasy, etc. Computational techniques, including accurate and computationally efficient models and optimization algorithms, may result in delimiting the performance limits of ABHs, and we hope that this work has contributed to this ultimate goal.

5. ACKNOWLEDGMENTS

The authors are grateful for financial support from GACR grant GA22-33896S. This work was supported by the Ministry of Education, Youth and Sports of the Czech Republic through the e-INFRA CZ (ID:90140).

6. REFERENCES

[1] M. A. Mironov and V. V. Pislyakov, "One-dimensional acoustic waves in retarding structures with propagation velocity tending to zero," *Acoust Phys*, vol. 48, pp. 347–352, 2002.

[2] O. Guasch, M. Arnela, and P. Sánchez-Martín, "Transfer matrices to characterize linear and quadratic acoustic black holes in duct terminations," *J Sound Vib*, vol. 395, pp. 65–79, 2017.

[3] O. Guasch, P. Sánchez-Martín, and D. Ghilardi, "Application of the transfer matrix approximation for wave propagation in a metafluid representing an acoustic black hole duct termination," *Appl Mathe Model*, vol. 77, pp. 1881–1893, 2020.

[4] A. A. El-Ouahabi, V. V. Krylov, and D. O'Boy, "Experimental investigation of the acoustic black hole for sound absorption in air," in *Proceedings of 22nd International Congress on Sound and Vibration, Florence, Italy*, 2015.

[5] A. A. El-Ouahabi, V. V. Krylov, and D. O'Boy, "Investigation of the acoustic black hole termination for sound waves propagating in cylindrical waveguides," in *Proceedings of the International Conference Inter-Noise 2015, San Francisco, USA*, 2015.

[6] M. A. Mironov and V. V. Pislyakov, "One-dimensional sonic black holes: Exact analytical solution and experiments," *J Sound Vib*, vol. 473, p. 115223, 2020.

[7] O. Umnova, D. Brooke, P. Leclaire, and T. Dupont, "Multiple resonances in lossy acoustic black holes–theory and experiment," *J Sound Vib*, vol. 543, p. 117377, 2023.

[8] N. Sharma, O. Umnova, and A. Moorhouse, "Low frequency sound absorption through a muffler with metamaterial lining," in *24th International Congress on Sound and Vibration 2017 (ICSV 24), London, UK*, 2017.

[9] X. Zhang and L. Cheng, "Broadband and low frequency sound absorption by sonic black holes with micro-perforated boundaries," *J Sound Vib*, vol. 512, p. 116401, 2021.

[10] Y. Mi, L. Cheng, W. Zhai, and X. Yu, "Broadband low-frequency sound attenuation in duct with embedded periodic sonic black holes," *J Sound Vib*, vol. 536, p. 117138, 2022.

[11] A. Mousavi, M. Berggren, and E. Wadbro, "How the waveguide acoustic black hole works: A study of possible damping mechanisms," *J Acoust Soc Am*, vol. 151, pp. 4279–4290, 2022.

[12] M. Červenka and M. Bednařík, "On the role of resonance and thermoviscous losses in an implementation of "acoustic black hole" for sound absorption in air," *Wave Motion*, vol. 114, p. 103039, 2022.

[13] N. Jiménez, V. Romero-García, V. Pagneux, and J.-P. Groby, "Rainbow-trapping absorbers: Broadband, perfect and asymmetric sound absorption by subwavelength panels for transmission problems," *Sci Rep*, vol. 7, p. 13595, 2017.

[14] M. Stinson, "The propagation of plane sound waves in narrow and wide circular tubes, and generalization to uniform tubes of arbitrary cross-sectional shape," *J Acoust Soc Am*, vol. 89, pp. 550–558, 1991.

[15] *Global Optimization Toolbox User's Guide, MATLAB R2020a,*. Natick, Massachusetts, USA: The MathWorks, Inc., 2020.